Measurement of the full shear-induced self-diffusion tensor of noncolloidal suspensions

V. Breedveld,[a] D. van den Ende,[b] M. Bosscher, R. J. J. Jongschaap, and J. Mellema
Rheology Group, Twente Institute of Mechanics, J.M.Burgerscentrum, Department of Applied Physics, University of Twente, P.O. Box 217, 7500 AE Enschede, the Netherlands

(Received 3 January 2002; accepted 22 March 2002)

The full diffusion tensor of shear-induced self-diffusion has been measured experimentally for the first time. In addition to the well-known components in the velocity gradient, D_{yy}, and vorticity direction, D_{zz}, the coefficients D_{xx} and D_{xy} have been determined for concentrated suspensions of noncolloidal hard spheres as a function of particle volume fraction. Owing to the shear-induced nature of the phenomenon, these four coefficients are the only nonzero elements of the diffusion tensor. The newly determined diffusion quantities have been obtained by extending our correlation based technique [J. Fluid Mech. **375**, 297 (1998); Phys. Rev. E **63**, 021403 (2001)] with a method to subtract convective displacements due to the shear flow. The diffusion in the velocity direction, D_{xx}, is almost an order of magnitude larger than the other components and the only nonzero off-diagonal component, D_{xy}, is negative and small compared to the diagonal components of the diffusion tensor. In principle the applied technique is also feasible for measuring other anisotropic diffusion mechanisms, e.g., Brownian diffusion in steady shear flow. © *2002 American Institute of Physics.* [DOI: 10.1063/1.1478770]

I. INTRODUCTION

Shear-induced self-diffusion is an important transport mechanism in noncolloidal suspensions under shear. The nature of the phenomenon is different from the more familiar Brownian diffusion in colloidal suspensions, which is caused by thermal fluctuations, and turbulent diffusion, driven by inertia. Shear-induced diffusion occurs even in case of high Péclet and low Reynolds numbers and is, in the case of hard spheres, the result of excluded volume effects only: neighboring particles are displaced from their initial streamline when passing each other. In a concentrated suspension these interactions lead to net displacements after completion of the interactions, as opposed to an isolated two-particle collision in Stokes flow, where the trajectories are purely symmetrical. It has been shown by a number of researchers[1–5] that, in a certain range of times, the displacements $\Delta\mathbf{r}$ scale diffusively with time: $\langle \Delta\mathbf{r}\Delta\mathbf{r}\rangle \propto 2\ \mathbf{D}\Delta t$, where $\langle\cdot\rangle$ denotes an ensemble average. The self-diffusion process can give rise to macroscopic particle migration in case of inhomogeneities in concentration and/or flow field, the so-called gradient diffusion,[6,7] which is of practical importance when handling suspensions under high Péclet and low Reynolds number conditions. In general, particles tend to accumulate in regions of low shear rate, i.e., the center of a Poiseuille flow geometry or at the outer cylinder wall of a Couette shear cell.

Recently it was shown experimentally[8] and also numerical studies[9,10] indicate that the stochastic motion of the particles is not diffusive on all time scales. Hence this process cannot be described by the convection diffusion equation used so far.[4,5,9] In this paper we concentrate on the stochastic motion of individual particles. We will study $\langle \Delta\mathbf{r}(t)\Delta\mathbf{r}(t)\rangle$ starting from a Langevin equation, including a stochastic force $\mathbf{F}_s(t)$ with colored noise properties, acting on the particle due to the hydrodynamic interactions with all other particles. The mean square displacements are determined by the ensemble averaged autocorrelation function of this stochastic force $\mathbf{G}(t-t')=\langle \mathbf{F}_s(t)\mathbf{F}_s(t')\rangle$. We will show that after sufficient long time the behavior will be diffusive, i.e., the self-diffusion tensor

$$\mathbf{D}=\frac{1}{2}\lim_{t\to\infty}\frac{d}{dt}\langle \Delta\mathbf{r}(t)\Delta\mathbf{r}(t)\rangle=\frac{1}{\zeta^2}\int_0^\infty \mathbf{G}(s)\,ds \tag{1}$$

is constant. Here ζ is the hydrodynamic friction factor of the particles.

Because the phenomenon is purely induced by the shear flow, dimensional analysis and symmetry considerations show that in simple shear flow the self-diffusion tensor has—by analogy with the stress tensor—the following form:[11,12]

$$\mathbf{D}\equiv \dot{\gamma}a^2\hat{\mathbf{D}}(\phi)=\dot{\gamma}a^2\begin{Bmatrix}\hat{D}_{xx} & \hat{D}_{xy} & 0\\ \hat{D}_{yx} & \hat{D}_{yy} & 0\\ 0 & 0 & \hat{D}_{zz}\end{Bmatrix}. \tag{2}$$

The Cartesian coordinate system is chosen according to the convention that x is along the velocity, y along the velocity gradient, and z along the vorticity direction. The diffusion tensor $\mathbf{D}$ is an isotropic function of the velocity gradient tensor $\mathbf{L}=\dot{\gamma}\mathbf{e}_x\mathbf{e}_y$. Hence the principle of frame indifference[13] prescribes the above-given form of $\mathbf{D}(\phi)$; $\hat{D}_{xy}$ and $\hat{D}_{yx}$ are the only off-diagonal components that could differ from zero.

[a]Present address: Department of Chemical Engineering, University of California, Santa Barbara, CA 93106-5080.
[b]Electronic mail: h.t.m.vandenEnde@tn.utwente.nl

Moreover from Eq. (1) and the symmetry of $\mathbf{G}(t-t')$ one observes that $\mathbf{D}$ is symmetric: $\hat{D}_{xy}=\hat{D}_{yx}$. The scaling can be understood by realizing that the reciprocal of the shear rate $\dot{\gamma}^{-1}$ and the particle radius a are the only relevant time and length scale of a system of noncolloidal hard spheres. $\hat{\mathbf{D}}$ is the dimensionless diffusion tensor which components depend only on the particle volume fraction ϕ.

Following the same arguments the autocorrelation tensor $\mathbf{G}(t-t')$ will scale with $(a\dot{\gamma}\zeta)^2$, where ζ is the friction factor of a particle in the fluid, and will have the same components different from zero as $\mathbf{D}$.

To date only experimental results have been reported on $\hat{D}_{yy}$ and $\hat{D}_{zz}$.[1–5] Since these experiments have shown that shear-induced diffusion is anisotropic ($\hat{D}_{yy}/\hat{D}_{zz}\approx 1.5$), knowledge of the full self-diffusion tensor is highly desirable for understanding the microhydrodynamics of concentrated suspensions. In this paper we present an approach to determine the remaining components $\hat{D}_{xx}$ and $\hat{D}_{xy}$. The technique is an extension of our previous work on measuring $\hat{D}_{yy}$ and $\hat{D}_{zz}$.[5] In Sec. II the analysis of the full diffusion tensor will be introduced from the experimental point of view. The mathematical framework is then provided in Sec. III. Results are presented in Sec. IV and Sec. V closes the paper with a discussion of the results and conclusions.

II. EXPERIMENT

A. Materials

For the experiments we used a well-defined size fraction of poly/methyl methacrylate (PMMA) particles with diameter 90 ± 15 μm (Lucite, class 4F, produced by ICI, density $\rho=1.172$ g/ml, refractive index $n_D=1.491$ at 25 °C). The suspending fluid consisted of a mixture of Triton X-100, demineralized water and zinc-II-chloride, which has been measured to be Newtonian at relevant shear rates with a viscosity of 3.4 Pa s (23 °C). The fluid composition was chosen such that it matched the density and refractive index of the particles as well as possible. A small fraction (typically 0.3% of the suspension volume) of the particles was colored with fabric dye to function as tracer particles. The density of the dyed particles was not notably affected: even after several weeks no separation of dyed and undyed particles could be observed in the suspensions. Samples were prepared at several particle volume fractions (20%–45%). Matching the physical properties of the particles and suspending fluid enables optical access, while sedimentation is eliminated.

The motion of the colored tracer particles in a counter-rotating large radius, narrow gap Couette geometry (details in Breedveld *et al.*[5]) is monitored by means of a digital CCD camera. The counter-rotating feature is required to keep tracer particles within the observation window sufficiently long to capture long-time shear-induced self-diffusion for dimensionless times $\dot{\gamma}\Delta t>1$. With this geometry we were able to observe an autocorrelation peak even for $\dot{\gamma}\Delta t=2.8$, compared to $\dot{\gamma}\Delta t=0.5$ in the non-counter-rotating setup.[4] The large radius (120 mm) and narrow gap (4 mm) design minimizes the influences of curvature and prevents migration due to gradient diffusion. The images are stored real-time in sequences of 200 images through a frame grabber (Matrox Pulsar) which is controlled by dedicated image grabbing software (Hispa). By repeating the grabbing procedure large image sets are obtained.

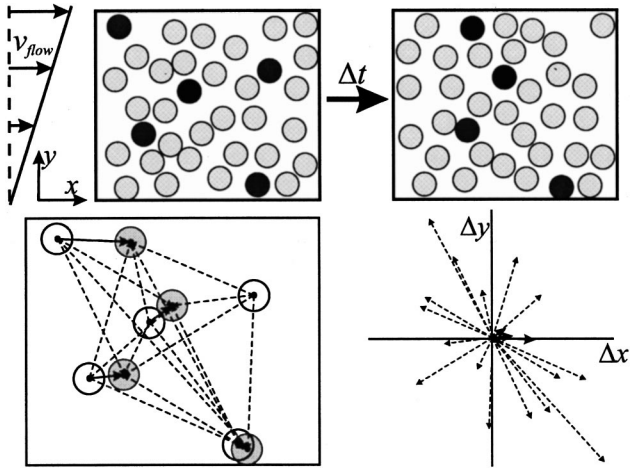

FIG. 1. Example of the correlation procedure; upper panel: two subsequent images of the suspension under shear; lower left: network of auto- (—) and cross-correlation (---) vectors; lower right: same set of vectors now pointing all from the same origin.

B. Method

The measuring technique is based on spatial correlation of tracer positions in a concentrated suspension under shear; this method we developed originally for measuring $\hat{D}_{yy}$ and $\hat{D}_{zz}$.[4,5] Following this approach, first all tracer positions are determined in the sequence of video images using commercial image analysis software (Optimas, Media Cybernetics). After obtaining the tracer positions, the actual correlation procedure is applied. The successive steps of this procedure are illustrated in Fig. 1.

The upper half of Fig. 1 displays two subsequent images in which a number of tracer particles appear as detected by the image analysis software. The macroscopic flow field is drawn on the left. The tracer positions in the first frame are correlated to all tracers in the second frame. For this particular example, the result is a set of $4\times 5=20$ correlation vectors, which are shown in the lower left-hand image. The dashed lines denote cross-correlation vectors between different particles and the solid vectors represent autocorrelation vectors. Only the latter contain information about particle motion. However, in the experimental situation the particle identity is *a priori* unknown when comparing pictures taken at relatively long time intervals, so that it is impossible to distinguish between cross- and autocorrelation vectors on the basis of the image sequence. However, for our correlation technique such knowledge is not required. Because of the different nature of cross- and autocorrelation vectors, statistical analysis of a large data set enables us to discriminate between the two types and extract information about particle motion. In the lower right quadrant of Fig. 1 the vectors are collected in a graph where they all point from the same origin. Due to the shear flow the autocorrelation vectors all

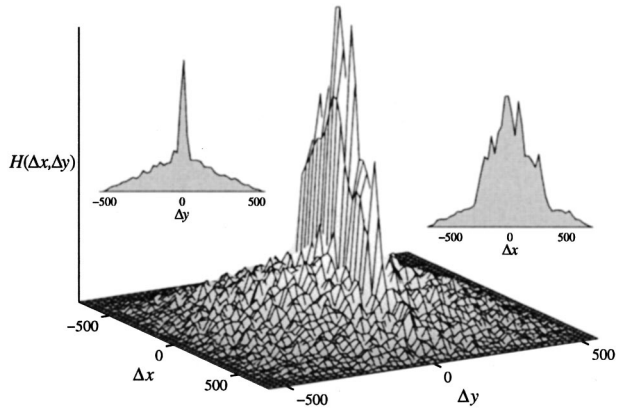

FIG. 2. Histogram of correlation vectors $(\Delta x,\Delta y)$ for a set of 8000 images at $\dot{\gamma}\Delta t=1.10$ and $\phi=0.35$; the units along the horizontal axes are pixels and H is given in arbitrary (non-normalized) units.

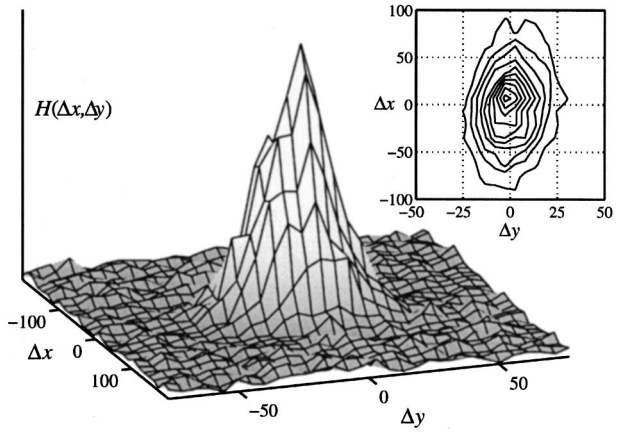

FIG. 3. Histogram of correlation vectors $(\Delta x,\Delta y)$ for the data set of Fig. 2; inset shows the contour lines of the central peak.

have a convective component to the right in addition to the stochastic component. Therefore they are all located in the area just to the right of the origin. The cross-correlations on the other hand are scattered all over the graph.

By repeating the correlation procedure for several thousand image combinations, a histogram like Fig. 2 can be built of the correlation vectors $(\Delta x,\Delta y)$. The insets depict projections of the histogram along the Δx and Δy axes. The histogram in Fig. 2 represents the experimental probability H to detect a correlation vector $(\Delta x,\Delta y)$, while observing the tracer particles along the vorticity (z) direction:

$$H(\Delta x,\Delta y)=F(\Delta x,\Delta y)[P_e(\Delta x,\Delta y)+C]. \tag{3}$$

It contains two separate contributions: a central peak $P_e(\Delta x,\Delta y)$ that consists of the autocorrelation vectors and a background C due to the cross-correlations. These are both multiplied by the detection efficiency $F(\Delta x,\Delta y)$ for a certain correlation vector $(\Delta x,\Delta y)$ to be observed; F is purely determined by the shape of the observation window and can be calculated as the convolution of the window with itself.[5,12] Essentially, F accounts for the fact that it is less likely to find a large displacement, compared to a small one, due to the finite size of the observation window.

The cross-correlation background C is directly related to the distribution of tracer particles over the observation window. At high volume fraction of particles one expects some structure in the pair distribution function $g(r)$ and thus in the distribution of tracer particles. However no structure could be observed in this distribution, not even when one correlates images with themselves $(\Delta t=0)$. This is due to the fact that a projection of the distribution (in this case along the vorticity direction) is observed. In this projection possible structures in the distribution will be averaged out. Therefore the background C is assumed to be constant at all values of Δt and further analysis can be concentrated on the autocorrelation peak which contains information about the motion of tracer particles.

The histogram clarifies why the measurement of D_{xx} and D_{xy} is more complicated than measurement of the other components: the stochastic displacements in the velocity direction (x) are masked by variations in the macroscopic velocity over the observation window (see v_{flow} in Fig. 1). Unlike the example of Fig. 1 where the shear flow gave a net displacement to the right, Fig. 2 contains experimental data taken in our counter-rotating geometry and thus the autocorrelation peak is centered around the origin: the average x displacement of all particles equals zero. However, the convective flow still varies as a function of y coordinate and because of this the central peak is much wider in the x than in the y direction.

The convective motion can be eliminated in a fairly simple way: since the macroscopic simple shear flow is stationary and the positions of tracer particles are known before performing the correlation step, the convective displacement $\Delta\mathbf{x}_c=(\frac{1}{2}\dot{\gamma}(y_0+y)+v_0)\Delta t\,\mathbf{e}_x$ can be subtracted. Here y_0 and $y=y_0+\Delta y$ denote the y component of the tracer position in, respectively, the first and second image of the correlated image pair.

Using the transformation $\Delta\mathbf{x}-\Delta\mathbf{x}_c\rightarrow\Delta\mathbf{x}$ where the latter $\Delta\mathbf{x}$ now represents only the stochastic part of the displacement, Fig. 2 changes to Fig. 3. Note from the scales along the axes that the central autocorrelation peak in Fig. 3 is now much narrower in the x direction; $P_e(\Delta x,\Delta y)$ is no longer broadened by variations in the convective flow over the observation window. The efficiency function $\tilde{F}(\Delta x,\Delta y)$ differs from F in Fig. 2 since the image window is slightly distorted by the applied transformation, but $\tilde{F}$ can still be calculated directly from the known geometry of the observation window after the above coordinate transformation has been performed. The cross-correlation term C is not affected by the transformation: it was independent of $(\Delta x,\Delta y)$ in the original situation and remains constant.

The contour plot of the peak in the inset of Fig. 3 now reveals important qualitative information about $\hat{D}_{xy}$: the main axes of the peak are tilted which indicates that $\hat{D}_{xy}\neq 0$. Taking into account that the shear flow in our experiment was applied in the negative x direction (see Fig. 4), it can be concluded that $\hat{D}_{xy}<0$. Physically this means that a particle undergoing a stochastic displacement in the $+x$ $(-x)$ direction most likely simultaneously moves in the $-y$ $(+y)$ direction.

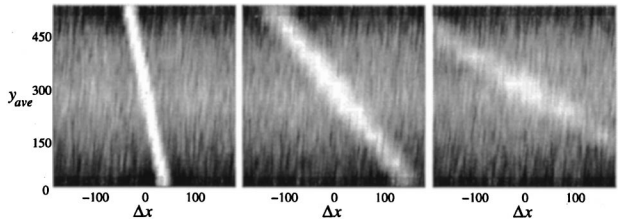

FIG. 4. Top view of three experimental histograms of correlation vectors Δx as a function of the average y position during the time interval, y_{ave}; data set is the same as for Fig. 2; from left to right the strain is, respectively, $\dot{\gamma}\Delta t = 0.14$, 0.55, and 1.10.

The shear flow parameters $\dot{\gamma}$ and v_0 needed for this convective motion subtraction are determined from the data set instead of using an external estimate based on the rotational speed of the Couette geometry. After calculation of the correlation vectors, a histogram can be built plotting the experimental probability of a displacement Δx at different y positions, using the average position $\frac{1}{2}(y_0+y)$ for the y position during the correlation time Δt. Examples of such a histogram are presented in Fig. 4. The top view of the histogram is shown and the height (probability) is coded in gray scales, lighter scales indicating higher probabilities. The autocorrelation vectors are located in the central peak (light band) in this figure as well. The center of the band represents the average displacement and thereby the velocity profile in the observation window. By performing a linear fit to these graphs, the parameters $\dot{\gamma}$ and v_0 were obtained.

In case of observation along the vorticity axis (e.g., Fig. 1) information about displacements in the z direction is lost and a two-dimensional distribution in the x–y plane is measured as in Fig. 3. In order to determine $\hat{D}_{zz}$ the particles should be observed along the gradient direction and the distribution in the x–y plane can be analyzed, as was done in a previous study.[5]

III. LANGEVIN EQUATION

Although the experimental method to remove the convective flow by using the average y position of the tracers is intuitive, a closer look at the theoretical implications of this coordinate transformation is required to justify the approach.

From experimental histograms like Fig. 3 values for $\langle \Delta x \Delta x \rangle$, $\langle \Delta x \Delta y \rangle$, and $\langle \Delta y \Delta y \rangle$ can be obtained. These can be compared directly to theoretical predictions. For a particle subjected to simple shear flow the following force balance or Langevin equation can be formulated:

$$\zeta(\mathbf{v}_0 + \mathbf{L}\cdot\mathbf{r}(t) - \mathbf{v}(t)) + \mathbf{F}_s(t) = 0, \tag{4}$$

where ζ is the hydrodynamic friction factor of the particles, $\mathbf{L} = \dot{\gamma}\,\mathbf{e}_x\mathbf{e}_y$ is the velocity gradient tensor, $\mathbf{v}_0 = v_0\,\mathbf{e}_x$ the flow velocity at $y=0$, and $\mathbf{F}_s(t)$ the stochastic force acting on the particle due to hydrodynamic interactions with all other particles in the fluid. This force is characterized by the following properties:

$$\begin{aligned} &\langle \mathbf{F}_s(t) \rangle = 0, \\ &\langle \mathbf{F}_s(t)\mathbf{F}_s(t') \rangle = \mathbf{G}(t-t'). \end{aligned} \tag{5}$$

The tensor $\mathbf{G}(s)$ is assumed to be symmetric: $\mathbf{G}(s) = \mathbf{G}^T(s)$. Moreover we assume that for large time differences $|t-t'|$ the autocorrelation of the force vanishes faster than with $|t-t'|^{-3}$, i.e., $\lim_{s\to\infty}(s^3\mathbf{G}(s)) = 0$. The solution of Eq. (4) can be found in[14]

$$\begin{aligned} \mathbf{r}(t) = \mathbf{r}_0 + (\mathbf{v}_0 + \mathbf{L}\cdot\mathbf{r}_0)t + \tfrac{1}{2}(\mathbf{L}\cdot\mathbf{v}_0)t^2 \\ + \frac{1}{\zeta}\int_0^t (\mathbf{I} + (t-t')\mathbf{L})\cdot\mathbf{F}_s(t')\,dt', \end{aligned} \tag{6}$$

where $\mathbf{I}$ is the unit tensor and $\mathbf{r}_0$ the position of the particle at $t=0$. The average displacements are now equal to

$$\begin{aligned} &\langle x - x_0 \rangle = \left(y_0 + \frac{v_0}{\dot{\gamma}} \right) \gamma, \\ &\langle y - y_0 \rangle = \langle z - z_0 \rangle = 0, \end{aligned} \tag{7}$$

where $\gamma = \dot{\gamma}\Delta t$. Using the transformation described in Sec. II B:

$$\begin{aligned} \Delta x &= x - x_0 - \gamma(y+y_0)/2, \\ \Delta y &= y - y_0, \\ \Delta z &= z - z_0, \end{aligned}$$

one obtains for the mean square displacements:

$$\begin{aligned} \frac{\langle \Delta x \Delta x \rangle}{2a^2} &= \gamma Q_{xx}^{(0)}(\gamma) - Q_{xx}^{(1)}(\gamma), \\ &\quad + \tfrac{1}{6}Q_{yy}^{(3)}(\gamma) - \tfrac{1}{4}\gamma^2 Q_{yy}^{(1)}(\gamma) + \tfrac{1}{12}\gamma^3 Q_{yy}^{(0)}(\gamma), \\ \frac{\langle \Delta x \Delta y \rangle}{2a^2} &= \gamma Q_{xy}^{(0)}(\gamma) - Q_{xy}^{(1)}(\gamma), \\ \frac{\langle \Delta y \Delta y \rangle}{2a^2} &= \gamma Q_{yy}^{(0)}(\gamma) - Q_{yy}^{(1)}(\gamma), \\ \frac{\langle \Delta z \Delta z \rangle}{2a^2} &= \gamma Q_{zz}^{(0)}(\gamma) - Q_{zz}^{(1)}(\gamma). \end{aligned} \tag{8}$$

Here the following definition has been used:

$$Q_{ij}^{(n)}(\gamma) = \int_0^\gamma q^n \hat{G}_{ij}(q)\,dq \tag{9}$$

with $\hat{G}_{ij}(\dot{\gamma}t) = G_{ij}(t)/(a\dot{\gamma}\zeta)^2$. In the limit for $\gamma\to\infty$ the coefficients $Q_{ij}^{(n)}(\gamma)$ become constant, due to the finite autocorrelation time of the stochastic force, while for $n=0$ they are related to the diffusion coefficients by

$$\hat{D}_{ij} = Q_{ij}^{(0)}(\infty). \tag{10}$$

From Eq. (8) one observes that, for sufficiently large values of γ, $\langle \Delta x \Delta y \rangle$, $\langle \Delta y \Delta y \rangle$, and $\langle \Delta z \Delta z \rangle$ indeed grow linearly with γ, showing an offset for $\gamma = 0$, but the behavior of $\langle \Delta x \Delta x \rangle$ is less obvious. However, $Q_{xx}^{(0)}(\infty)$ can be determined from

$$\lim_{\gamma\to\infty}\frac{d}{d\gamma}\frac{\langle\Delta x\Delta x\rangle}{2a^2}=Q_{xx}^{(0)}(\infty)-\frac{1}{2}\gamma Q_{yy}^{(1)}(\infty)+\tfrac{1}{4}\gamma^2 Q_{yy}^{(0)}(\infty), \tag{11}$$

where $Q_{yy}^{(0)}(\infty)$ is the slope of $\langle\Delta y\Delta y\rangle/(2a^2)$ plotted against the strain γ for $\gamma\to\infty$ and $Q_{yy}^{(1)}(\infty)$ is determined by extrapolating the linear part of this curve toward $\gamma=0$.

For a fully diffusive process (i.e., on all time scales) the autocorrelation function is given by: $\mathbf{G}(s)=\mathbf{H}\,\delta(s)$ where $\delta(s)$ is the Dirac delta function and $\mathbf{H}$ a symmetric tensor whose coefficients are constant. In that case $\mathbf{Q}^{(n)}=0$ for $n>0$, while $\mathbf{Q}^{(0)}=\hat{\mathbf{D}}$, independent of γ, so Eq. (8) reduces to the mean square displacements of particles diffusing in a simple shear flow.[14]

IV. RESULTS

For a quantitative analysis of the diffusion coefficients we check the time dependence of Eq. (8). The quantities $\langle\Delta x^2\rangle$, $\langle\Delta y^2\rangle$, and $\langle\Delta x\Delta y\rangle$ can be determined directly by calculating

$$\langle\Delta r_i\Delta r_j\rangle=\int\int(\Delta r_i\Delta r_j)\,P_e(\Delta x,\Delta y)\,d\Delta x\,d\Delta y$$

from the experimentally obtained autocorrelation peak P_e in Fig. 3. In this procedure we have to take into account that the experimental distribution contains an unknown constant cross-correlation contribution C and a known geometrical prefactor $\tilde{F}$ [Eq. (3)]. Therefore the histogram must be divided by the efficiency function $\tilde{F}$ before the calculation is done, even if the variations of this function are very small in the neighborhood of the autocorrelation peak, as can be seen in Fig. 3.

By measuring $\langle\Delta x^2\rangle$, $\langle\Delta y^2\rangle$, and $\langle\Delta x\Delta y\rangle$ for various values of the dimensionless time $\gamma=\dot{\gamma}\Delta t$ the diffusive scaling can be checked. Here it is important to notice that, for sufficiently large values of $\dot{\gamma}\Delta t$, Eq. (8) reveals three contributions to $\langle\Delta x^2\rangle$: one diffusive term that grows linearly with time and two terms that grow with $(\dot{\gamma}\Delta t)^2$ and $(\dot{\gamma}\Delta t)^3$, respectively. This is caused by diffusion in the y direction, followed by convection along a different streamline in the x direction.

Figure 5 shows the averages of Eq. (8) as a function of $\dot{\gamma}\Delta t$ for a particle volume fraction of 0.45. The averages are made dimensionless with the particle radius squared, a^2. Note that two scales have been used in order to capture the information in a single graph. To obtain the diffusion coefficient D_{xx} from the slope of the curve, $\langle\Delta x^2\rangle/a^2-C$ has been plotted against $\dot{\gamma}\Delta t$, where C is defined by: $C=\frac{1}{12}(\dot{\gamma}\Delta t)^2(\langle\Delta y^2\rangle+2\langle\Delta y^2\rangle_0)/a^2$. $\langle\Delta y^2\rangle_0$ is the extrapolation of the linear part of the $(\langle\Delta y^2\rangle,\dot{\gamma}\Delta t)$ curve toward $\dot{\gamma}\Delta t=0$.

The evolution of the mean square displacements is for $1<\dot{\gamma}\Delta t<3$ well-described by linear fits, so the process can indeed be described as diffusive. The diffusion coefficients are calculated as half the slope of the fitted lines. From these observations one may conclude that the autocorrelation time

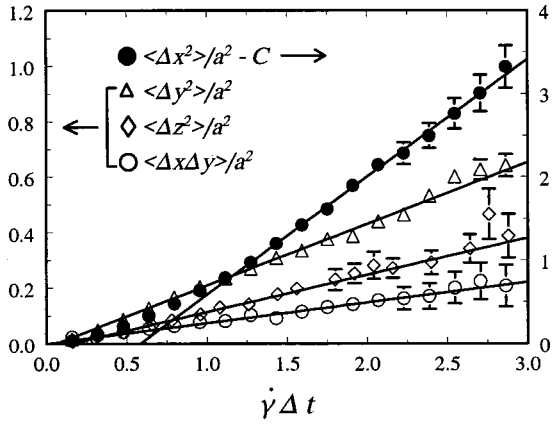

FIG. 5. Evolution of the averages of Eq. (8) with dimensionless time $\dot{\gamma}\Delta t$ for a suspension with $\phi=0.45$. The lines represent the linear fits for $\dot{\gamma}\Delta t>1$; $C=(1/12a^2)\,(\dot{\gamma}\Delta t)^2(\langle\Delta y^2\rangle+2\langle\Delta y^2\rangle_0)$; note the different scale used for $\langle\Delta x^2\rangle$.

of the stochastic hydrodynamic force is of the order of $\dot{\gamma}^{-1}$. For $\dot{\gamma}\Delta t<1$ the averages scale nonlinearly with time; the motion of the particles is nondiffusive as was expected from Eq. (8). The measured $\langle\Delta\mathbf{r}\Delta\mathbf{r}\rangle$ dependence on $\dot{\gamma}\Delta t$ in this regime can be related to the velocity autocorrelation function:

$$\langle v_i(0)v_j(t)\rangle=\frac{1}{\zeta^2}G_{ij}(t)=\frac{1}{2}\frac{d^2}{dt^2}\langle\Delta r_i\Delta r_j\rangle, \tag{12}$$

where the index pair $\{ij\}$ can be $\{xy\}$, $\{yy\}$, or $\{zz\}$. For $\langle v_x(0)v_x(t)\rangle$ the situation is more complicated due to the convective part of the velocity in this direction.

In Fig. 6 the coefficients of shear-induced self-diffusion as obtained in this study are combined with the results of our previous work[5] to provide information on the full diffusion tensor as a function of particle volume fraction. As was already noticed qualitatively in Fig. 3, the diffusion in the velocity direction (x) is an order of magnitude larger than in the other directions, while the off-diagonal component $\hat{D}_{xy}$ is negative and of the same magnitude as the components $\hat{D}_{yy}$ and $\hat{D}_{zz}$.

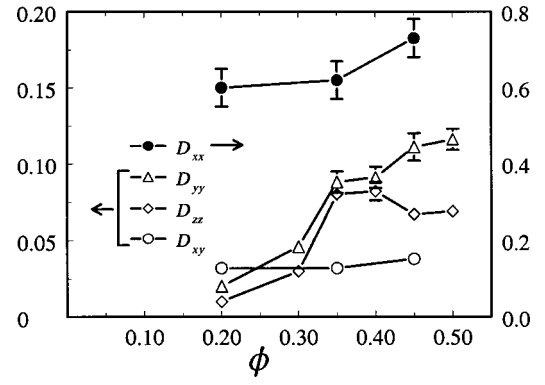

FIG. 6. Dimensionless coefficients of shear-induced self-diffusion $\hat{D}_{ij}$ as a function of particle volume fraction ϕ; note that a different scale has been used for $\hat{D}_{xx}$.

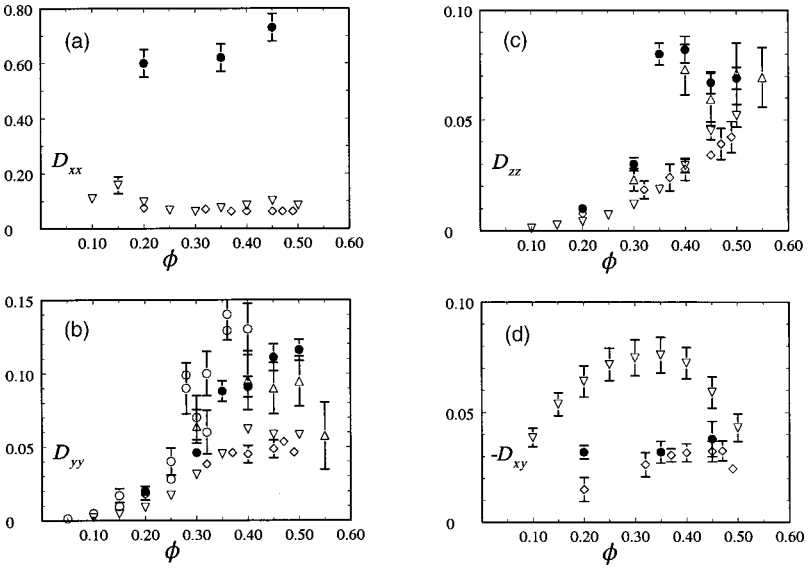

FIG. 7. The coefficients $\hat{D}_{xx}$ (a), $\hat{D}_{yy}$ (b), $\hat{D}_{zz}$ (c), and $\hat{D}_{xy}$ (d) as a function of volume fraction; (△) represent data from Ref. 3, (○) data from Ref. 6, (◇) numerical data from Ref. 9, and (∇) from Ref. 16, while (●) were measured in this study.

V. DISCUSSION AND CONCLUSION

In contrast to the earlier measured D_{yy} and D_{zz} both D_{xx} and D_{xy} do not significantly vary with volume fraction over the available data range. These are, to our best knowledge, the first experimental data on the full diffusion tensor. Recently, however, these quantities have been determined in numerical calculations using the Stokesian dynamics method.[15] In this study it was also found that D_{xy} is negative. Moreover, the authors give a physical explanation for the negative D_{xy} value, based on the two particle pair distribution function at high Péclet numbers where hydrodynamics dominates the process. In a second study from this group[9] it was found that at low volume fractions the value for D_{xx} is significantly larger than those of D_{yy} or D_{zz}. Their results show however a decrease of D_{xx} with increasing volume fraction. That D_{xx} is significantly larger than D_{yy} or D_{zz} is in keeping with a theoretical study of Acrivos *et al.*[16] They argued that at low volume fractions D_{yy} and D_{zz} should grow with ϕ^2 but they predicted that D_{xx} grows with $\phi \ln \phi^{-1}$ due to a divergence in $\langle \Delta x^2 \rangle$ in an isolated two particle collision for $\phi \to 0$. This divergence is rendered finite due to the fact that the slow collisions, causing the divergence, are cutoff by occasional collisions with other particles. This leads to the nondivergent ϕ dependence, given previously. Hence for low volume fractions D_{xx} is expected to be significantly larger than D_{yy} and D_{zz}. Their values, however, are lower than ours; e.g., a factor 4 at $\phi = 0.2$.

For comparison the numerical results mentioned previously[9,15] are given in Fig. 7 together with the available experimental results from us and other researchers.[1–3] Although the scattering is large, the experimental results are in reasonable agreement with each other. The numerical results, however, are systematically smaller than the experimental results, typically a factor 2, but for D_{xx} it is about a factor 6. Sierou and Brady[9] explain this from their observation that the autocorrelation time of the stochastic force is not of the order $(1/\dot{\gamma})$ but $(10/\dot{\gamma})$, which means that our measurements were done for to small strains $\dot{\gamma}\Delta t$. This is, however, in contradiction with the observations of Leighton and Acrivos[2] and Phan and Leighton[3] which were done at much larger strains $\dot{\gamma}\Delta t > 10$. To settle the discussion on this point it should be worthwhile to extend the measurements to larger strains. At the moment this is not possible due to limitations in the experimental method of which the nonperfect optical density matching is the most important; the particles are slightly inhomogeneous and so matching can not be improved.

To describe our data we used a Langevin approach to evaluate the problem of the nondiffusive short time scales. This approach has shown to be useful, however other approaches are possible. Sierou and Brady[9] start with a modified master equation for the displacement probability function resulting in time dependent diffusion coefficients. Both approaches give the same description of the diffusive behavior for large strains, $\dot{\gamma}\Delta t \gg 1$, resulting in the same expressions for the long time diffusion coefficients, but for small strains, $\dot{\gamma}\Delta t \ll 1$, the nondiffusive behavior is treated different.

In conclusion, for time scales $\dot{\gamma}\Delta t > 1$ the average squared displacements $\langle \Delta \mathbf{r} \Delta \mathbf{r} \rangle$ scale with $a^2 \dot{\gamma}\Delta t$ so the process is indeed diffusive. The stochastic part of the particle motion is anisotropic and concentration dependent; D_{zz} and D_{yy} strongly increase with volume fraction ϕ, while D_{xx} and D_{xy} show hardly any ϕ dependence. D_{xx} is almost one order of magnitude larger than the other components of $\mathbf{D}$ and D_{xy} is negative. For shorter time scales the stochastic part of the particle motion can be separated from the convective motion, too. On these time scales the measured $\langle \Delta \mathbf{r} \Delta \mathbf{r} \rangle$ provides information about the velocity autocorrelation function, which will be subject of further research.

ACKNOWLEDGMENT

This work has been supported by the Foundation for Fundamental Research on Matter (FOM), which is financially supported by the Netherlands Organization for Scientific Research (NWO).

[1] E. Eckstein, D. Bailey, and A. Shapiro, J. Fluid Mech. **79**, 191 (1977).
[2] D. Leighton and A. Acrivos, J. Fluid Mech. **181**, 415 (1987).
[3] S. Phan and D. Leighton, J. Fluid Mech. (submitted).
[4] V. Breedveld, D. van den Ende, A. Tripathi, and A. Acrivos, J. Fluid Mech. **375**, 297 (1998).
[5] V. Breedveld, D. van den Ende, M. Bosscher, R. J. J. Jongschaap, and J. Mellema, Phys. Rev. E **63**, 021403 (2001).
[6] D. Leighton and A. Acrivos, J. Fluid Mech. **177**, 109 (1987).
[7] A. Acrivos, J. Rheol. **39**, 813 (1995).
[8] V. Breedveld, D. van den Ende, R. J. J. Jongschaap, and J. Mellema, J. Chem. Phys. **114**, 5923 (2001).
[9] A. Sierou and J. F. Brady, J. Fluid Mech. (submitted).
[10] G. Drazer, J. Koplik, B. Khusid, and A. Acrivos, J. Fluid Mech. (submitted).
[11] J. Morris and J. F. Brady, J. Fluid Mech. **312**, 223 (1996).
[12] V. Breedveld, Ph.D. thesis, University of Twente, The Netherlands, 2000.
[13] W. R. Schowalter, *Mechanics of Non-Newtonian Fluids* (Pergamon, Oxford, 1978).
[14] J. K. G. Dhont, *An Introduction to Dynamics of Colloids* (Elsevier, Amsterdam, 1996).
[15] D. Foss and J. F. Brady, J. Fluid Mech. **401**, 243 (1999).
[16] A. Acrivos, G. K. Batchelor, E. J. Hinch, D. L. Koch, and R. Maury, J. Fluid Mech. **240**, 651 (1992).